

Robust Actuator Fault Diagnosis Algorithm for Autonomous Hexacopter UAVs^{*}

Antonio Gonzalez Rot^{*}, Agus Hasan^{*}, and
Poramate Manoonpong^{**}

^{*} Center for Unmanned Aircraft Systems
University of Southern Denmark
5230 Odense, Denmark
(e-mails: goant18@student.sdu.dk, agha@mmmi.sdu.dk).
^{**} Embodied AI and Neurorobotics Lab
University of Southern Denmark
5230 Odense, Denmark
(e-mail: poma@mmmi.sdu.dk).

Abstract: This paper presents a robust actuator fault diagnosis algorithm for hexacopter Unmanned Aerial Vehicles (UAVs). The algorithm, based on Adaptive eXogenous Kalman Filter (AXKF), consists of two-stage operations: (i) a nonlinear observer and (ii) a linearized adaptive Kalman filter. To this end, we provide a sufficient condition for the nonlinear observer and recursive formulas for the linearized adaptive Kalman filter. The algorithm is tested for actuator fault diagnosis of a hexacopter UAV. Simulation results show that the proposed cascaded algorithm is able to accurately estimate the magnitude of the actuator fault.

Keywords: Fault diagnosis, Kalman filter, Unmanned Aerial Vehicles (UAVs).

1. INTRODUCTION

1.1 Motivation

Autonomous systems such as autonomous Unmanned Aerial Vehicles (UAVs) can cause harm or injury for people and other adverse consequences, especially when they are flying Beyond Visual Line Of Sight (BVLOS). In this case, it is very important to increase their reliability, e.g., to detect failures and to react to them in the safest and fastest possible way. Due to mechanical vibrations, high temperature, and heavy workload, the actuator system of an autonomous UAV is prone to failure. In general, there are two ways to increase the reliability of UAVs: hardware redundancy and analytical redundancy. The idea of the first approach is to add redundant hardware, e.g., sensors or actuators. However this comes with a cost, since the system gets heavier, more expensive, and more complex. The second approach is to use analytical models for fault diagnosis, which does not require additional hardware. Therefore, it is well suited for UAVs, where space is limited and additional weight results in a shorter flight time.

1.2 Literature review

Fault diagnosis consists of three stages: detection, isolation, and estimation. Studies have been conducted on this issue by using adaptive methods, such as Adaptive Extended Kalman filter (AEKF) for UAV fault di-

agnosis based on online modification of noise matrices (Zerdali (2019), Hajiyev and Soken (2013)). However, such a method cannot be used to calculate the magnitude of the fault, which is useful for fault-tolerant control. To overcome this problem, Amoozgar et al. (2013); Kim et al. (2009); Moghadam and Caliskan (2015) have focused on adaptive two-stage extended Kalman filters. This method allows to measured the failure if there is sensory feedback for fault measurement.

For a linear system, it has been possible to detect actuator loss of effectiveness using Adaptive Kalman Filter (AKF) (Zhang (2018), Wu et al. (1998), Skriver et al. (2019)). Nevertheless, this method cannot be directly applied to nonlinear systems. Linearizing the nonlinear systems may cause the estimations do not converged to the actual values. To solve this problem different approaches have been taken into account. For example, Yang et al. (2013) have used Unscented Kalman Filter (UKF) using a deterministic sampling approach. Safarinejadian and Kowsari (2014) have extended this by combining the Unscented and Extended Kalman filters with Gaussian processes for fault detection and residual evaluation.

1.3 Contribution of this paper

All methods mentioned above, while impressive in their own right, have not addressed the magnitude estimation of the actuator fault of complex nonlinear systems, like hexacopter UAVs, with high accuracy. This is an important factor for safety. From this point of view, we propose here a new approach for actuator fault diagnosis of hexacopter UAVs. This approach consist of two-stage operations: (i)

^{*} This work was supported by the Free the Drones (FreeD) project, partly funded by Innovation Fund Denmark, at Center for Unmanned Aircraft Systems, Mærsk Mc-Kinney Møller Institute, University of Southern Denmark, project number 5156-00008B.

a nonlinear observer, which is used to guarantee the estimation converging to the actual values; (ii) a linearized AKF, which is used to remove the noises and to estimate the magnitude of the fault.

2. PROBLEM STATEMENT

Let us consider dynamic models of hexacopter UAVs that can be written in the following form

$$\mathbf{x}(k+1) = \mathbf{A}\mathbf{x}(k) + \mathbf{f}(\mathbf{x}(k)) + \mathbf{B}\mathbf{u}(k) + \Phi(k)\boldsymbol{\vartheta} + \mathbf{w}(k) \quad (1)$$

$$\mathbf{y}(k) = \mathbf{C}\mathbf{x}(k) + \mathbf{v}(k) \quad (2)$$

where $\mathbf{x}(k) \in \mathbb{R}^n$ is the state vector, $\mathbf{A} \in \mathbb{R}^{n \times n}$ is the state matrix, $\mathbf{f} : \mathbb{R}^n \rightarrow \mathbb{R}^n$ is the nonlinear function, $\mathbf{B} \in \mathbb{R}^{n \times l}$ is the input matrix, $\mathbf{u}(k) \in \mathbb{R}^l$ is the input vector, $\mathbf{y}(k) \in \mathbb{R}^m$ is the output vector, and $\mathbf{C} \in \mathbb{R}^{m \times n}$ is the measurement matrix. The term $\Phi(k)\boldsymbol{\vartheta}$ represents actuator faults with a known matrix sequence $\Phi(k) \in \mathbb{R}^{n \times p}$ and a constant (or piecewise constant with rare jumps) parameter vector $\boldsymbol{\vartheta} \in \mathbb{R}^p$. The process and measurement noise are denoted by $\mathbf{w}(k)$ and $\mathbf{v}(k)$, respectively. These noises are assumed to be zero mean Gaussian white noise with known covariance matrices, i.e., $\mathbf{w}(k) \sim (0, \mathbf{Q}_F(k))$, $\mathbf{v}(k) \sim (0, \mathbf{R}_F(k))$.

An example of actuator faults represented by the term $\Phi(k)\boldsymbol{\vartheta}$ is the loss of actuator effectiveness. In this case, when $p = l$, the matrix sequence $\Phi(k)$ is given by $\Phi(k) = -\mathbf{B}\text{diag}(\mathbf{u}(k))$. Thus, when the faults happen the nominal control term $\mathbf{B}\mathbf{u}(k)$ is given by $\mathbf{B}(\mathbf{I}_l - \text{diag}(\boldsymbol{\vartheta}))\mathbf{u}(k)$. In this case, if $\text{diag}(\boldsymbol{\vartheta}) = \mathbf{I}_l$, then the actuators experience complete failures, while if $\text{diag}(\boldsymbol{\vartheta}) = \mathbf{0}$, then there is no failure.

The following assumptions are used throughout this paper.

Assumption 1. The matrices \mathbf{A} , \mathbf{B} , \mathbf{C} , $\Phi(k)$, $\mathbf{Q}_F(k)$, and $\mathbf{R}_F(k)$ are upper bounded.

Assumption 2. The nonlinear function \mathbf{f} is one-sided Lipschitz, i.e., there exists $\rho \in \mathbb{R}$ such that

$$\langle \mathbf{f}(\mathbf{x}_1) - \mathbf{f}(\mathbf{x}_2), \mathbf{x}_1 - \mathbf{x}_2 \rangle \leq \rho \|\mathbf{x}_1 - \mathbf{x}_2\|^2 \quad (3)$$

Assumption 3. The nonlinear function \mathbf{f} satisfies the quadratic inner-boundedness condition, i.e., there exist scalar $\beta, \eta \in \mathbb{R}$ such that

$$\Delta \mathbf{f}^\top \Delta \mathbf{f} \leq \beta \|\mathbf{x}_1 - \mathbf{x}_2\|^2 + \eta \langle \mathbf{x}_1 - \mathbf{x}_2, \Delta \mathbf{f} \rangle \quad (4)$$

where $\Delta \mathbf{f} = \mathbf{f}(\mathbf{x}_1) - \mathbf{f}(\mathbf{x}_2)$.

The problem of actuator fault diagnosis is to estimate the state vector $\mathbf{x}(k)$ and the fault parameter $\boldsymbol{\vartheta}$ from the measurement vector $\mathbf{y}(k)$ under process and measurement noise $\mathbf{w}(k)$ and $\mathbf{v}(k)$.

3. ACTUATOR FAULT DIAGNOSIS ALGORITHM

In this section, we present a robust actuator fault diagnosis algorithm based on Adaptive eXogenous Kalman Filter (AXKF). The algorithm consists of two-stage estimations: (i) a nonlinear observer, (ii) a linearized Adaptive Kalman Filter. Let $\bar{\mathbf{x}}(k+1)$ denotes the state estimation from the

nonlinear observer, while $\hat{\mathbf{x}}(k+1)$ and $\hat{\boldsymbol{\vartheta}}(k+1)$ denote the state and fault estimation from the linearized Adaptive Kalman Filter. The schematic diagram of the algorithm is presented in Fig. 1.

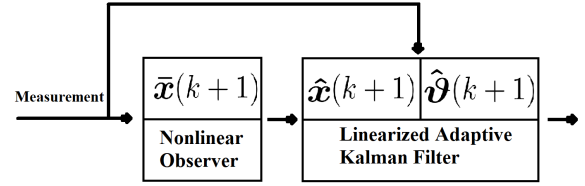


Fig. 1. The schematic diagram of AXKF for actuator fault diagnosis.

3.1 Nonlinear Observer

The nonlinear observer is designed as follow

$$\bar{\mathbf{x}}(k+1) = \mathbf{A}\bar{\mathbf{x}}(k) + \mathbf{f}(\bar{\mathbf{x}}(k)) + \mathbf{B}\mathbf{u}(k) + \Phi(k)\boldsymbol{\vartheta} + \mathbf{G}^{-1}\mathbf{Y}\check{\mathbf{y}}(k) \quad (5)$$

where $\check{\mathbf{x}}(k) = \mathbf{x}(k) - \bar{\mathbf{x}}(k)$, $\check{\mathbf{y}}(k) = \mathbf{y}(k) - \mathbf{C}\bar{\mathbf{x}}(k)$, and $\Delta \mathbf{f}(\check{\mathbf{x}}(k)) = \mathbf{f}(\mathbf{x}(k)) - \mathbf{f}(\bar{\mathbf{x}}(k))$. In this case, we assume the fault parameter $\boldsymbol{\vartheta}$ can be obtained from the second stage estimation. The error dynamic is given by

$$\check{\mathbf{x}}(k+1) = (\mathbf{A} - \mathbf{G}^{-1}\mathbf{Y}\mathbf{C})\check{\mathbf{x}}(k) + \Delta \mathbf{f}(\check{\mathbf{x}}(k)) \quad (6)$$

Theorem 1. If there exist a symmetric positive definite matrix $\mathbf{G} \in \mathbb{R}^{n \times n}$ and a matrix $\mathbf{Y} \in \mathbb{R}^{n \times m}$ such that

$$\begin{pmatrix} -\mathbf{G} + a_1\mathbf{I}_n & \mathbf{L}^\top\mathbf{G} + a_2\mathbf{I}_n & \mathbf{L}^\top\mathbf{G} \\ \mathbf{G}\mathbf{L} + a_3\mathbf{I}_n & \mathbf{G} + a_4\mathbf{I}_n & \mathbf{0}_n \\ \mathbf{G}\mathbf{L} & \mathbf{0}_n & -\mathbf{G} \end{pmatrix} < \mathbf{0} \quad (7)$$

where $\mathbf{L} = \mathbf{A} - \mathbf{G}^{-1}\mathbf{Y}\mathbf{C}$, $a_1 = \epsilon_1\rho + \epsilon_2\beta$, $a_2 = a_3 = \frac{\eta\epsilon_2 - \epsilon_1}{2}$, and $a_4 = -\epsilon_2$, for ϵ_1, ϵ_2 and $\rho, \beta, \eta \in \mathbb{R}$, then the equilibrium $\check{\mathbf{x}} = \mathbf{0}$ of the error dynamic (6) is globally uniformly asymptotically stable.

Proof 1. Let us define

$$V(k) = \check{\mathbf{x}}(k)^\top \mathbf{G} \check{\mathbf{x}}(k) \quad (8)$$

Furthermore, let $\Delta V_k = V(k+1) - V(k)$. Thus, we have

$$\Delta V_k = \check{\mathbf{x}}(k+1)^\top \mathbf{G} \check{\mathbf{x}}(k+1) - \check{\mathbf{x}}(k)^\top \mathbf{G} \check{\mathbf{x}}(k) \quad (9)$$

Let $\mathbf{L} = \mathbf{A} - \mathbf{G}^{-1}\mathbf{Y}\mathbf{C}$. Substituting (6) into (9), yields

$$\Delta V_k \leq \check{\mathbf{x}}(k)^\top (\mathbf{L}^\top \mathbf{G} \mathbf{L} - \mathbf{G}) \check{\mathbf{x}}(k) + 2\check{\mathbf{x}}(k)^\top \mathbf{L}^\top \mathbf{G} \Delta \mathbf{f}(\check{\mathbf{x}}(k)) + \Delta \mathbf{f}(\check{\mathbf{x}}(k))^\top \mathbf{G} \Delta \mathbf{f}(\check{\mathbf{x}}(k)) \quad (10)$$

Thus, we have

$$\Delta V_k \leq \begin{pmatrix} \check{\mathbf{x}} \\ \Delta \mathbf{f} \end{pmatrix}^\top \begin{pmatrix} \mathbf{L}^\top \mathbf{G} \mathbf{L} - \mathbf{G} + \nu \mathbf{I}_n & \mathbf{L}^\top \mathbf{G} \\ \mathbf{G} \mathbf{L} & \mathbf{G} \end{pmatrix} \begin{pmatrix} \check{\mathbf{x}} \\ \Delta \mathbf{f} \end{pmatrix} \quad (11)$$

From Assumption 2, we obtain $\Delta V_k \leq 0$ if

$$\begin{pmatrix} \mathbf{L}^\top \mathbf{G} \mathbf{L} - \mathbf{G} + a_1\mathbf{I}_n & \mathbf{L}^\top \mathbf{G} + a_2\mathbf{I}_n \\ \mathbf{G} \mathbf{L} + a_3\mathbf{I}_n & \mathbf{G} + a_4\mathbf{I}_n \end{pmatrix} < \mathbf{0} \quad (12)$$

Applying Schur complement completes the proof.

3.2 Linearized Adaptive Kalman Filter

Linearizing (1) at $\bar{\mathbf{x}}(k)$, we obtain

$$\mathbf{x}(k+1) = \mathbf{F}(\bar{\mathbf{x}}(k))\mathbf{x}(k) + \mathbf{E}(\bar{\mathbf{x}}(k)) + \mathbf{B}\mathbf{u}(k) + \Phi(k)\boldsymbol{\vartheta} + \mathbf{w}(k) \quad (13)$$

where

$$\mathbf{F}(\bar{\mathbf{x}}(k)) = \mathbf{A} + \left. \frac{\partial \mathbf{f}(\mathbf{x}(k))}{\partial \mathbf{x}(k)} \right|_{\bar{\mathbf{x}}(k)} \quad (14)$$

$$\mathbf{E}(\bar{\mathbf{x}}(k)) = \mathbf{f}(\bar{\mathbf{x}}(k)) - \left. \frac{\partial \mathbf{f}(\mathbf{x}(k))}{\partial \mathbf{x}(k)} \right|_{\bar{\mathbf{x}}(k)} \bar{\mathbf{x}}(k) \quad (15)$$

From here, we use Adaptive Kalman Filter Algorithm for actuator fault diagnosis developed by Zhang (2018). A summary of the algorithm can be found in Table 1.

3.3 Adaptive eXogenous Kalman Filter Algorithm (AXKF)

The stability of the cascaded system has been studied by Loria and Panteley (2004) (see, Theorem 2.1 and Proposition 2.3). Furthermore, a similar concept for discrete-time systems has been proposed by Hasan (2019); Hasan et al. (2019b,a) and for continuous systems by Gudmundsson et al. (2018); Hasan and Johansen (2018). The algorithm is a combination of the two-stage operations described above: (i) a nonlinear observer and (ii) a linearized adaptive Kalman filter. In the first stage, the state estimation is obtained after calculating the observer gains \mathbf{G} and \mathbf{Y} . In the second stage, the Kalman gain and the fault estimation gain are obtained from the error covariance matrix. One important assumption is the signals in the matrix $\Phi(k)$ are persistently exciting in the sense that there exist an integer $N > 0$ and a real constant α such that, for all integer k , the matrix sequence $\Omega(k)$ satisfy

$$\sum_{s=0}^{N-1} \Omega^\top(k+s)\Sigma^{-1}(k+s)\Omega(k+s) \geq \alpha \mathbf{I}_p \quad (16)$$

4. DYNAMIC MODEL OF A HEXACOPTER



Fig. 2. Image of a hexacopter DJI F550, similar to the system simulated.

In this section, we present a dynamic model used to describe a hexacopter (see Fig. 2). The classical dynamic model is based on a Euler-Lagrange equation

$$\mathbf{M}(\mathbf{q})\ddot{\mathbf{q}} + \mathbf{C}(\mathbf{q}, \dot{\mathbf{q}})\dot{\mathbf{q}} + \frac{\partial \mathcal{V}(\mathbf{q})}{\partial \mathbf{q}} = \mathbf{B}\mathbf{u} + \Phi\boldsymbol{\vartheta} \quad (17)$$

where \mathbf{q} is the orientation around the x , y , and z axis (ϕ , θ , ψ), \mathcal{V} is the potential energy function, \mathbf{B} is the input matrix, and $\boldsymbol{\vartheta}$ is the actuator gain loss. The generalized inertia matrix $\mathbf{M}(\mathbf{q})$ and the Coriolis term $\mathbf{C}(\mathbf{q}, \dot{\mathbf{q}})$ are given by

$$\mathbf{M}(\mathbf{q}) = \mathbf{R}(\mathbf{q})\mathbf{J}\mathbf{R}^T(\mathbf{q}) \quad (18)$$

$$\mathbf{C}(\mathbf{q}, \dot{\mathbf{q}}) = \dot{\mathbf{M}}(\mathbf{q}) - \frac{1}{2} \frac{\partial \dot{\mathbf{q}}^T \mathbf{M}(\mathbf{q})}{\partial \mathbf{q}} \quad (19)$$

with

$$\mathbf{J} = \begin{bmatrix} I_{xx} & 0 & -I_{xz} \\ 0 & I_{yy} & 0 \\ -I_{xz} & 0 & I_{zz} \end{bmatrix} \quad (20)$$

$$\mathbf{R}(\mathbf{q}) = \begin{bmatrix} 1 & 0 & 0 \\ 0 & \cos \phi & -\sin \phi \\ -\sin \theta & \sin \theta \cos \theta & \cos \phi \cos \theta \end{bmatrix} \quad (21)$$

Here, I_{xx} , I_{yy} , I_{zz} I_{xz} are the moment of inertia around the specific axis.

Applying Port-Controlled Hamiltonian model (PCH) (Ortega et al. (2002), Acosta et al. (2005)) the Euler-Lagrange equation can be transformed into the following form

$$\begin{bmatrix} \dot{\mathbf{q}} \\ \dot{\mathbf{p}} \end{bmatrix} = \begin{bmatrix} 0 & \mathbf{I}_n \\ -\mathbf{I}_n & 0 \end{bmatrix} \begin{bmatrix} \nabla_{\mathbf{q}} \mathbf{H} \\ \nabla_{\mathbf{p}} \mathbf{H} \end{bmatrix} + \begin{bmatrix} 0 \\ \mathbf{B} \end{bmatrix} \mathbf{u} + \begin{bmatrix} 0 \\ \Phi \end{bmatrix} \boldsymbol{\vartheta} \quad (22)$$

where $\mathbf{p} = \mathbf{M}(\mathbf{q})\dot{\mathbf{q}}$ is the generalized momenta and the Hamiltonian function

$$\mathbf{H}(\mathbf{q}, \mathbf{p}) = \frac{1}{2} \mathbf{p}^T \mathbf{M}^{-1}(\mathbf{q})\mathbf{p} + \mathcal{V}(\mathbf{q}) \quad (23)$$

represent the total energy of the system. Applying time discretization using Euler method, the Euler-Lagrange equation (22) can be transformed into (1), with $\mathbf{A} = \mathbf{I}_6$.

In the particular case of a hexacopter attitude control, two different approaches can be considered:

- Virtual control input where the desired moments around each axis is the control signal:
 $\mathbf{u} = [M_x \ M_y \ M_z]^T$ and $\mathbf{B} = \mathbf{I}_3$
- Real control input where each motor is controlled individually:

$$\mathbf{u} = [T_1 \ T_2 \ T_3 \ T_4 \ T_5 \ T_6]^T \text{ and } \mathbf{B} = \begin{bmatrix} -L & 0 & -b \\ L & 0 & b \\ L \cos 60 & L \sin 60 & -b \\ -L \cos 60 & -L \sin 60 & b \\ -L \cos 60 & L \sin 60 & b \\ L \cos 60 & -L \sin 60 & -b \end{bmatrix}$$

Here, L is the distance from the propeller to the center of mass, 60 is the angle between the arm and the y axis and b is the drag coefficient of the propeller. The parameters of the hexacopter are shown in Table 2.

5. SIMULATION RESULTS

In this section, we describe simulation environment used for the numerical simulation where the effectiveness of the proposed algorithm is tested.

Table 1. Discrete-time AXKF algorithm for actuator fault diagnosis.

Initialization $\hat{\mathbf{x}}(0) = \hat{\mathbf{x}}_0, \hat{\boldsymbol{\vartheta}}(0) = \hat{\boldsymbol{\vartheta}}_0, \mathbf{P}(0 0) = \mathbf{P}_0, \boldsymbol{\Upsilon}(0) = \mathbf{0}, \mathbf{S}(0) = \mathbf{I}_p$
Determine observer gains \mathbf{G} and \mathbf{Y} based on Theorem 1
Recursions for $k = 0, 1, 2, \dots$
<i>First stage estimation: Nonlinear observer</i>
$\bar{\mathbf{x}}(k+1) = \mathbf{A}\bar{\mathbf{x}}(k) + \mathbf{f}(\bar{\mathbf{x}}(k), \mathbf{y}(k)) + \mathbf{B}\mathbf{u}(k) + \Phi(k)\bar{\boldsymbol{\vartheta}}(k) + \mathbf{G}^{-1}\mathbf{Y}\tilde{\mathbf{y}}(k)$
<i>Second stage estimation: Linearized Adaptive Kalman Filter</i>
Calculate the Kalman gain $\mathbf{K}(k+1)$ and error covariance matrix $\mathbf{P}(k+1 k+1)$
$\mathbf{P}(k+1 k) = \mathbf{F}(\bar{\mathbf{x}}(k))\mathbf{P}(k k)\mathbf{F}(\bar{\mathbf{x}}(k))^\top + \mathbf{Q}_F(k)$
$\boldsymbol{\Sigma}(k+1) = \mathbf{C}\mathbf{P}(k+1 k)\mathbf{C}^\top + \mathbf{R}_F(k)$
$\mathbf{K}(k+1) = \mathbf{P}(k+1 k)\mathbf{C}^\top\boldsymbol{\Sigma}(k+1)^{-1}$
$\mathbf{P}(k+1 k+1) = [\mathbf{I}_n - \mathbf{K}(k+1)\mathbf{C}]\mathbf{P}(k+1 k)$
Calculate the fault estimation gain $\boldsymbol{\Gamma}(k+1)$
$\boldsymbol{\Upsilon}(k+1) = (\mathbf{I}_n - \mathbf{K}(k+1)\mathbf{C})\mathbf{F}(\bar{\mathbf{x}}(k))\boldsymbol{\Upsilon}(k) + (\mathbf{I}_n - \mathbf{K}(k+1)\mathbf{C})\Phi(k)$
$\boldsymbol{\Omega}(k+1) = \mathbf{C}\mathbf{F}(\bar{\mathbf{x}}(k))\boldsymbol{\Upsilon}(k) + \mathbf{C}\Phi(k)$
$\boldsymbol{\Lambda}(k+1) = [\lambda\boldsymbol{\Sigma}(k+1) + \boldsymbol{\Omega}(k+1)\mathbf{S}(k)\boldsymbol{\Omega}(k+1)^\top]^{-1}$
$\boldsymbol{\Gamma}(k+1) = \mathbf{S}(k)\boldsymbol{\Omega}(k+1)^\top\boldsymbol{\Lambda}(k+1)$
$\mathbf{S}(k+1) = \frac{1}{\lambda}\mathbf{S}(k) - \frac{1}{\lambda}\mathbf{S}(k)\boldsymbol{\Omega}(k+1)^\top\boldsymbol{\Lambda}(k+1)\boldsymbol{\Omega}(k+1)\mathbf{S}(k)$
Calculate the measurement error $\tilde{\mathbf{y}}(k+1)$
$\tilde{\mathbf{y}}(k+1) = \mathbf{y}(k+1) - \mathbf{C}[\mathbf{f}(\bar{\mathbf{x}}(k)) + \mathbf{B}\mathbf{u}(k) + \Phi(k)\hat{\boldsymbol{\vartheta}}(k)]$
Calculate the state estimation $\hat{\mathbf{x}}(k+1)$ and fault estimation $\hat{\boldsymbol{\vartheta}}(k+1)$
$\hat{\boldsymbol{\vartheta}}(k+1) = \hat{\boldsymbol{\vartheta}}(k) + \boldsymbol{\Gamma}(k+1)\tilde{\mathbf{y}}(k+1)$
$\hat{\mathbf{x}}(k+1) = \mathbf{A}\hat{\mathbf{x}}(k) + \mathbf{f}(\hat{\mathbf{x}}(k)) + \mathbf{B}\mathbf{u}(k) + \Phi(k)\hat{\boldsymbol{\vartheta}}(k) + \mathbf{K}(k+1)\tilde{\mathbf{y}}(k+1) + \boldsymbol{\Upsilon}(k+1)[\hat{\boldsymbol{\vartheta}}(k+1) - \hat{\boldsymbol{\vartheta}}(k)]$

Table 2. System description.

\mathbf{I}_{xx}	0.0145
\mathbf{I}_{yy}	0.0141
\mathbf{I}_{zz}	0.0266
\mathbf{I}_{xz}	0
Arm length (L)	0.55
Propeller drag coefficient (b)	0.1

5.1 Simulation environment

The simulations are done in Matlab. In this case, the faults are introduced at different time steps. The sensor feedback in the simulation is computed from the real model and then used for the state and fault estimation. In this simulation, we assume the only sensor feedback available is the attitude of the hexacopter.

5.2 Numerical simulation

The model used in the simulation is based on the PCH dynamic model of the hexacopter with the implementation of the Adaptive eXogenous Kalman Filter algorithm. We assume only \mathbf{q} can be measured and we can control each motor individually. Thus, the model for this setup can be described as follow:

$$\mathbf{x} = \begin{bmatrix} \mathbf{q} \\ \mathbf{p} \end{bmatrix} \quad (24)$$

$$\mathbf{f}(\mathbf{x}) = \begin{bmatrix} 0 & \mathbf{I}_3 \\ -\mathbf{I}_3 & 0 \end{bmatrix} \begin{bmatrix} \nabla_{\mathbf{q}}\mathbf{H} \\ \nabla_{\mathbf{p}}\mathbf{H} \end{bmatrix} \quad (25)$$

$$\mathbf{C} = [\mathbf{I}_3 \ \mathbf{0}_3] \quad (26)$$

The fault $\boldsymbol{\vartheta}$ is defined as the actuator gain loss for each of the motors. Thus, in this case $\boldsymbol{\vartheta} \in \mathbb{R}^6$. If parameters in Theorem 1 are chosen as follow: $\epsilon_1 = 10$, $\epsilon_2 = 10$, $\eta = 1$, $\beta = -4$, $\rho = 1$, then we can choose $\mathbf{G} = 9 \cdot \mathbf{I}_6$ and $\mathbf{Y} = [3 \cdot \mathbf{I}_3 \ \mathbf{0}_3]^\top$, such that (7) is satisfied. Furthermore, the values of the noise covariance matrices are $\mathbf{Q}_F = 0.01 \cdot \mathbf{I}_6$ and $\mathbf{R}_F = 0.04 \cdot \mathbf{I}_3$, the initial states are $\hat{\mathbf{x}}(0) = \mathbf{0}$, $\mathbf{P}(0) = \mathbf{I}_6$, $\hat{\boldsymbol{\vartheta}}(0) = \mathbf{0}$, $\mathbf{S}(0) = 0.001 \cdot \mathbf{I}_6$ and the forgetting factor is $\lambda = 0.995$.

The system is simulated for 8 seconds with a time step of 1 millisecond. At the beginning, all the motors are stopped and after 1 second they are turn on to a constant thrust (Figure 3). Assuming a balanced system, the drone will takeoff with constant speed and maintain balance in the air. As the mass of the drone is not being taken into account this value is smaller than it should be, but it is good enough for simulation purpose. The motor fault occurs after 3.5 seconds on motor 1 going from 0 to 0.124 and after 5.5 seconds on motor 3 going from 0 to 0.135 (Figure 4). The red dash line represents the estimation, the blue and the black solid one show the observer output and the real value.

Based on the motor configuration shown in Figure 5, a gain loss on motor 1 will cause the UAV to be unbalanced in a positive angle around the x axis generating a moment around the same axis. In a similar way this will make the UAV to rotate around its z axis in a positive angle due to the total moment around the same axis generate by the drag of the propellers will be unbalanced.

Likewise, when the motor 3 has a fault, the moment around the x axis is reduced as the other side is also failing.

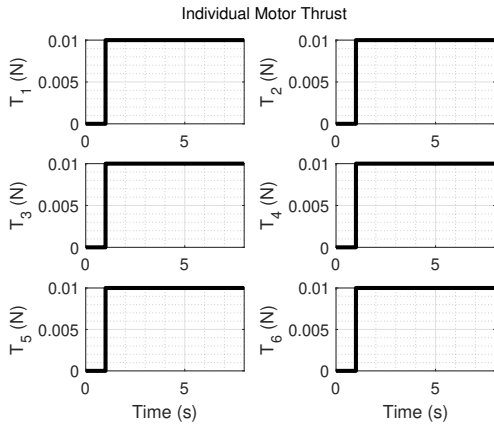


Fig. 3. Individual Thrust given by each motor. $t < 1 \rightarrow T_i = 0$, $t > 1 \rightarrow T_i = 0.01$.

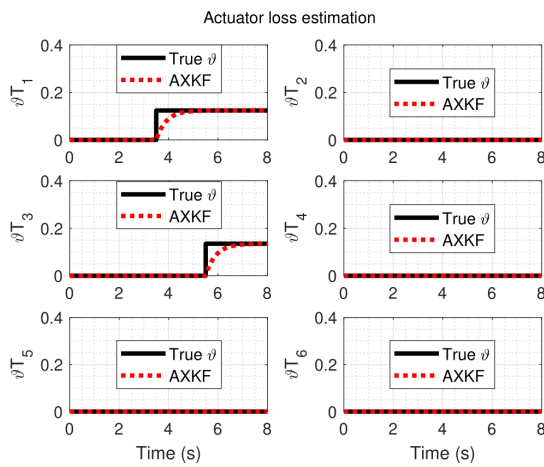


Fig. 4. Comparison between the estimated value of the fault and the actual value.

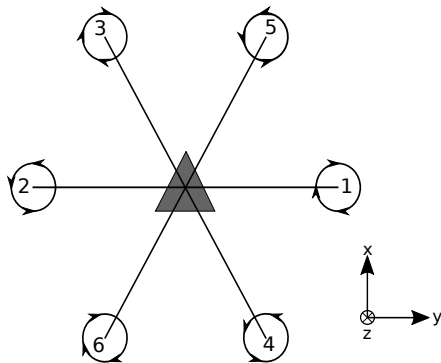


Fig. 5. Motor distribution and UAV coordinate system used for the simulation

However, the moment around the z axis is increased as both propellers are rotating in the direction generating a similar moment. Nevertheless, in this case the failure is not align within the y axis so the moment around it is lower than 0 making the drone tilt. These results can be seen in Figure 6 and 7. On the other hand, these figures also shown that the moments estimation has a slower dynamic than the attitude estimation due to the lack of sensory feedback on the moments estimation, thus it is necessary to estimate the fault in order to compensate it. For this

reason when the fault estimation is removed (Figure 8 and 9), it is no longer possible to estimate the moments.

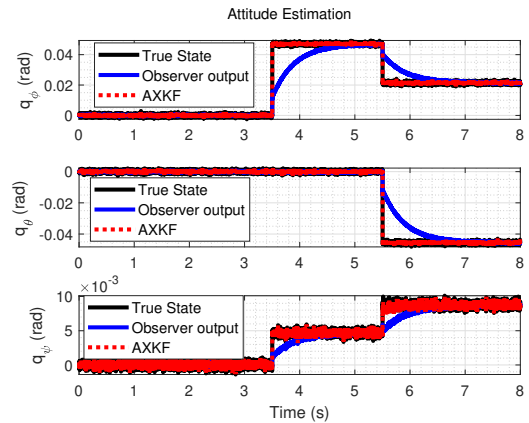


Fig. 6. q estimation ($q_\phi := \text{roll}$, $q_\theta := \text{pitch}$, $q_\psi := \text{yaw}$).

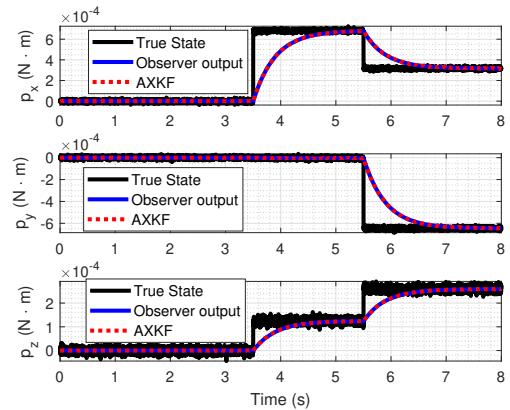


Fig. 7. p estimation ($p_x := \text{moment around the } x \text{ axis}$, $p_y := \text{moment around the } y \text{ axis}$, $p_z := \text{moment around the } z \text{ axis}$).

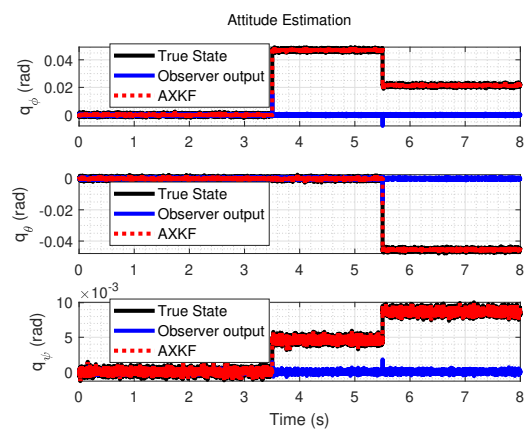


Fig. 8. q estimation ($q_\phi := \text{roll}$, $q_\theta := \text{pitch}$, $q_\psi := \text{yaw}$).

6. CONCLUSION

We present a new approach for actuator fault diagnosis of hexacopter UAVs. The state and fault estimation are guaranteed to converge to the actual value. Simulation

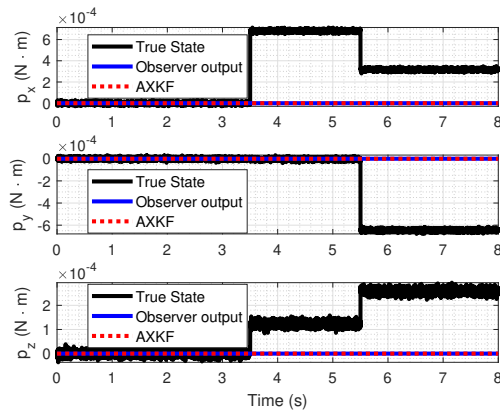


Fig. 9. p estimation (p_x := moment around the x axis, p_y := moment around the y axis, p_z := moment around the z axis).

results show our proposed algorithm can be used to estimate hexacopter actuator faults accurately. Further works include implementation of the actuator fault algorithm on a real hexacopter UAV.

REFERENCES

- Acosta, J.A., Ortega, R., Astolfi, A., and Mahindrakar, A.D. (2005). Interconnection and damping assignment passivity-based control of mechanical systems with underactuation degree one. *IEEE Transactions on Automatic Control*, 50(12), 1936–1955.
- Amoozgar, M.H., Chamseddine, A., and Zhang, Y. (2013). Experimental test of a two-stage kalman filter for actuator fault detection and diagnosis of an unmanned quadrotor helicopter. *Journal of Intelligent & Robotic Systems*, 70(1), 107–117. doi:10.1007/s10846-012-9757-7.
- Gudmundsson, V., Kristinsson, H., Petersen, S., and Hasan, A. (2018). Robust uav attitude estimation using a cascade of nonlinear observer and linearized kalman filter. In *ASME Dynamic Systems and Control Conference*.
- Hajiyev, C. and Soken, H.E. (2013). Robust adaptive kalman filter for estimation of uav dynamics in the presence of sensor/actuator faults. *Aerospace Science and Technology*, 28(1), 376 – 383. doi:https://doi.org/10.1016/j.ast.2012.12.003.
- Hasan, A. (2019). Adaptive exogenous kalman filter for actuator fault diagnosis in robotics and autonomous systems. In *International Conference on Control, Mechanics and Automation*.
- Hasan, A. and Johansen, T.A. (2018). Model-based actuator fault diagnosis in multirotor uavs. In *International Conference on Unmanned Aircraft Systems*, 1017–1024.
- Hasan, A., Skriver, M., and Johansen, T.A. (2019a). exogenous kalman filter for state-of-charge estimation in lithium-ion batteries. In *IEEE Conference on Control Technology and Applications*.
- Hasan, A., Tofterup, V., and Jensen, K. (2019b). Model-based fail-safe module for autonomous multirotor uavs with parachute systems. In *International Conference on Unmanned Aircraft Systems*, 406–412.
- Kim, K.H., Lee, J.G., and Park, C.G. (2009). Adaptive two-stage extended kalman filter for a fault-tolerant ins-gps loosely coupled system. *IEEE Transactions on Aerospace and Electronic Systems*, 45(1), 125–137. doi:10.1109/TAES.2009.4805268.
- Loria, A. and Panteley, E. (2004). *Cascaded nonlinear timevarying systems: analysis and design*. Springer-Verlag, London.
- Moghadam, M. and Caliskan, F. (2015). Actuator and sensor fault detection and diagnosis of quadrotor based on two-stage kalman filter. In *2015 5th Australian Control Conference (AUCC)*, 182–187.
- Ortega, R., Spong, M.W., Gomez-Estern, F., and Blankenstein, G. (2002). Stabilization of a class of underactuated mechanical systems via interconnection and damping assignment. *IEEE Transactions on Automatic Control*, 47(8), 1218–1233. doi:10.1109/TAC.2002.800770.
- Safarinejadian, B. and Kowsari, E. (2014). Fault detection in non-linear systems based on gp-ekf and gp-ukf algorithms. *Systems Science & Control Engineering*, 2(1), 610–620. doi:10.1080/21642583.2014.956843.
- Skriver, M., Helck, J., and Hasan, A. (2019). Adaptive extended kalman filter for actuator fault diagnosis. In *IEEE International Conference on System Reliability and Safety*, 406–412.
- Wu, N.E., Youmin Zhang, and Kemin Zhou (1998). Control effectiveness estimation using an adaptive kalman estimator. In *Proceedings of the 1998 IEEE International Symposium on Intelligent Control (ISIC) held jointly with IEEE International Symposium on Computational Intelligence in Robotics and Automation (CIRA) Intell*, 181–186. doi:10.1109/ISIC.1998.713657.
- Yang, X., Warren, M., Arain, B., Upcroft, B., Gonzalez, F., and Mejias, L. (2013). A ukf-based estimation strategy for actuator fault detection of uass. In *2013 International Conference on Unmanned Aircraft Systems (ICUAS)*, 516–525. doi:10.1109/ICUAS.2013.6564728.
- Zerdali, E. (2019). Adaptive extended kalman filter for speed-sensorless control of induction motors. *IEEE Transactions on Energy Conversion*, 34(2), 789–800. doi:10.1109/TEC.2018.2866383.
- Zhang, Q. (2018). Adaptive kalman filter for actuator fault diagnosis. *Automatica*, 93, 333 – 342.